Author's Accepted Manuscript

X-ray ionization differential ion mobility spectrometry

Andriy Kuklya, Tobias Reinecke, Florian Uteschil, Klaus Kerpen, Stefan Zimmermann, Ursula Telgheder

www.elsevier.com/locate/talanta

PII: S0039-9140(16)30769-X
DOI: http://dx.doi.org/10.1016/j.talanta.2016.10.024
Reference: TAL16944

To appear in: *Talanta*

Received date: 18 August 2016
Revised date: 22 September 2016
Accepted date: 2 October 2016

Cite this article as: Andriy Kuklya, Tobias Reinecke, Florian Uteschil, Klaus Kerpen, Stefan Zimmermann and Ursula Telgheder, X-ray ionization differential ion mobility spectrometry, *Talanta,* http://dx.doi.org/10.1016/j.talanta.2016.10.024

X-ray ionization differential ion mobility spectrometry

Andriy Kuklya[1*], Tobias Reinecke[2*], Florian Uteschil[1], Klaus Kerpen[1], Stefan Zimmermann[2], Ursula Telgheder[1,3]

[1]Department of Instrumental Analytical Chemistry, University of Duisburg-Essen (UDE), Universitätsstraße 5, 45141 Essen, Germany

[2]Department of Sensors and Measurement Technology, Institute of Electrical Engineering and Measurement Technology, Leibniz Universität Hannover, Appelstr. 9A, 30167 Hannover, Germany

[3]IWW Water Centre, Moritzstr. 26, 45476 Mülheim a.d. Ruhr, Germany

email: andriy.kuklya@uni-due.de

email: reinecke@geml.uni-hannover.de

***Corresponding Author:** , Tel : +49(0)201 183-6786, fax: +49(0)201 183-6773

***Corresponding Author.** Tel.: +49 (0)511 762-4228

Abstract

X-ray was utilized as an ionization source for differential ion mobility spectrometry (DMS) for the first time. The utilization of this ionization source increases the potential of DMS system for on-site based applications. The influence of experimental parameters (e.g. accelerating voltage, filament current, and separation field) on the analysis of model compounds was investigated and discussed. It was found that both the positive and the negative reactive ion peaks [RIP(+) and RIP(-)] formed during X-ray ionization are identical with those observed with the traditional ^{63}Ni radioactive ion source. This is especially notable for RIP(-), because the chemistry provided by other nonradioactive sources in the negative mode is more complicated or even different than that observed with a ^{63}Ni source. Increase of either filament current or accelerating voltage resulted in increased intensity of both RIP(+) and RIP(-). However, because of the materials used for construction of X-ray adapter the maximal level of filament current and accelerating voltage used in this study were limited to 700 mA and 5 kV, respectively. Analytical performance was determined with two model compounds (acetone and methyl salicylate) using X-ray and directly compared to ^{63}Ni ionization source. When X-ray was coupled to DMS, calculated LOD values were found to be within the range of 0.17 to 1.52 ppb v/v (concentration in the carrier gas). These values are competitive with those calculated for DMS equipped with traditional ^{63}Ni radioactive ionization source. The obtained results are promising enough to ensure the potential of X-ray as ionization source for DMS.

Keywords: Differential ion mobility spectrometry (DMS); High field asymmetric waveform ion mobility spectrometry (FAIMS); Chemical ionization (CI); X-ray ionization; ^{63}Ni ionization; On-site monitoring.

1. Introduction

Differential ion mobility spectrometry (DMS), often referred to as planar high-field asymmetric waveform ion mobility spectrometry (FAIMS), is a rapidly advancing technology. It is a technique that is both sensitive and fast, operates at atmospheric pressure, and provides a unique type of selectivity, which is orthogonal to most of other separation techniques [1,2].

In contrast to the conventional time-of-flight ion mobility spectrometry (TOF-IMS), in which the separation of ions is based on specific coefficients of ion mobility in a uniform electric field, separation of ions in DMS is based on a nonlinear dependence of the mobility coefficient to the electric field strength. This dependence can be explained by the field dependent reversible cluster formation model, which describes the field dependent variation of the average ion cluster cross section [3]. The fundamental principles of DMS can be found elsewhere [4,5].

DMS has found some applications as a stand-alone analyzer (with and without GC pre-separation) as well as a fast pre-separation technique for atmospheric pressure ionization mass spectrometry [2,6]. The separation based on ion mobility is fast as compared to chromatographic methods, namely provides separation on the *ms* to *s* time scale. Furthermore, DMS is able to separate isomeric and isobaric compounds. It was demonstrated that the methods based on ion mobility can significantly enhance the chromatographic separation or even be considered as an alternative to the chromatography [7,8]. The employment of DMS prior to mass spectrometer improves both selectivity and signal to noise ratio of MS measurement [9,10]. In many of DMS-based applications, the choice of the proper ionization source is a crucial step for the whole analytical procedure. Therefore, the understanding of the ionization processes and the developing of ion sources with high ion yield at environmental conditions cannot be overstated. The most frequently used ionization sources for DMS analysis of gaseous samples are radioactive sources (e.g. ^{63}Ni, ^{241}Am) [5,11], photoionization (Kr) [5,12], plasma-based sources (e.g. corona

discharge, low temperature plasma) [13,14]. However, the ionization mechanism provided by UV-photoionization differ with that provided by chemical ionization sources (e.g. corona or ^{63}Ni), and therefore may result different ions [10]. The difference in ionization pathway was also found between ionization by radioactive sources and by corona discharge operated in the negative mode (negative ions). The reactant ion chemistry provided by pulsed corona discharge in the negative mode is more complicated than that observed with a ^{63}Ni source [15]. The formation of the negative ions was found to be dependent on the experimental conditions, e.g. discharge power, gating time, geometry, and gas composition [10,16,17]. Depending on the strength of the electric field around the corona needle, formation of product ions may occur via different reactions (e.g. electron impact, photoionization and proton-transfer). Therefore, the recorded spectra may be rather complex and differ from those obtained with ^{63}Ni ionization [18]. Additional disadvantages are the reduced sensitivity provided by photoionization and the erosion of discharge electrode during the corona discharge resulting in degradation in performance of corona ionization source [19]. The main disadvantage of other plasma-based methods is that they are not widely commercially available.

The most commonly used ionization source in DMS is radioactive ^{63}Ni. This ionization source provides a very stable ion yield without an additional power source. Nevertheless, the use of this source is problematic for some applications due to regulatory problems associated with radioactive ionization sources (e.g. transportation, waste disposal, and safety regulations). These restrictions are particularly important for the devices intended to be used in the field. Therefore, the interest in replacing radioactive ionization source by nonradioactive alternatives has grown in recent years.

In the past, X-ray ionization was used successfully as ionization source for time-of-flight ion mobility spectrometry (TOF-IMS) [20,21]. The achieved spectra were equivalent to those

observed using ^{3}H-radioactive source. Another attractive feature of X-ray source is the possibility to adjust the radiation intensity by varying the experimental parameters, e.g. filament current and accelerating voltage. However, no applications of X-ray as ionization source for differential ion mobility spectrometry (DMS) or high field asymmetric waveform ion mobility spectrometry (FAIMS) can be found in literature.

In this work, the utilization of X-ray as an ionization source for differential ion mobility spectrometry has been introduced for the first time. The influence of main parameters, e.g. accelerating voltage and filament current, was investigated. Additionally, the X-ray ionization source was compared with traditional for differential ion mobility spectrometry radioactive ^{63}Ni ionization source.

2. Experimental section

2.1 Experimental setup.

The principle scheme of the experimental setup used in this study is shown in Fig. S-1 (see supporting information, top). In all experiments, the carrier gas was purified air (dew point -85°C) at a constant flow rate of 300 mL min^{-1}. The purified air was selected as a carrier gas to simulate the expected environment in the field experiments. The carrier gas with desired concentration of model compounds was prepared by mixing the purified air with an additional flow of sample gas in the required proportion. The individual flows were controlled by mass flow controllers (MFC, LOW-ΔP-FLOW, Bronkhorst Mättig GmbH, Germany). The sample gas flow was prepared by passing of the purified air flow through a vapor generator (VG) equipped with a permeation tube oven (Model 150 Dynacalibrator, Vici Metronics, USA). The concentration of model compounds in the carrier gas was calculated using the weight loss of the permeation tube over a certain time. The overall carrier gas flow was additionally controlled by a flow meter

(MFM, FP-407, Applied Instruments, Netherlands) located on the exhaust of DMS. Pressure was monitored using the pressure sensor from the DMS, which is built on the input to the analyzer.

The X-ray source was connected with DMS over the home-made adapter (see supporting information, Fig. S-1, bottom). The adapter was assembled onto the DMS lamp holder instead of the original photoionization lamp.

2.2 X-ray source.

A commercially available miniature X-ray source (XRT-50-Rh-0.6-125, Newton Scientific, Inc., USA) with continuous power rating of 2 W was used in this study. Thus, an additional power supply is required. The X-ray source has a rhodium target with 0.6 μm thickness, tungsten filament, beryllium output window with 125 μm thickness, and a focal spot size of 1 mm x 2 mm. The maximum filament current and voltage are 0.9 A and 1.7 V, respectively. The operating voltage and the X-ray tube current ranges are 4 - 50 kV and 0 - 100 μA, respectively.

The high-voltage current was found to be dependent on both the filament current and the acceleration voltage. Increase of both the filament current and the acceleration voltage resulted in increase of the high-voltage current. In measurement presented in current work, the high-voltage current was within the range of 30-190 μA.

2.3 DMS.

Two differential ion mobility spectrometers of similar construction were utilized in this study. One is equipped with removable photoionization source (SVAC-UV, krypton 10.0/10.6 eV, Sionex Corp., USA). Another is equipped with radioactive ^{63}Ni ionization source (SVAC-V, ^{63}Ni 185 MBq, Sionex Corp., USA). DMS settings were as follows: sensor temperature = 80 °C, number of steps = 100, step duration = 10 ms, step settle time = 3 ms, steps to blank = 1. Samples were analyzed in the positive (positive ions) and negative (negative ions) modes at purified air

flow rate of 300 mL min^{-1}, unless otherwise noted. Compensating voltage range was set from -30 to +5 V.

For each sample, three single measurements were recorded using Sionex Expert software (version 2.4.0). For the determination of peak parameters (centre, height, FWHM), data were analyzed by the fityk (version 0.9.8) program [22]. Peaks were fitted with Gaussian functions using the Levenberg-Marquardt algorithm.

It should be noted that the analyte signal positions on the compensation voltage scale are very sensitive to even minor pressure differences. To enable comparison of spectra obtained under different pressures, the method described by Nazarov et al. was used [23]. This method proposes utilization of the reduced compensation field scale (CF, E/N) in Townsend units [Td] instead of the compensation voltage scale (CV, in [V]). This method was used in our previous studies and has shown to be able to minimize but not completely eliminate the differences between the peak positions in compensation field scale at different pressures. Therefore, the data presented in this manuscript were recorded within the narrow pressure gap between 14.40 and 14.55 psi.

2.4 Chemicals.

To verify the proposed method two model substances, namely acetone [Sigma Aldrich, > 99.8 %] and methyl salicylate [Sigma Aldrich, > 99 %], were selected. These substances are well investigated by differential ion mobility technique and were previously analyzed by time of flight ion mobility spectrometry coupled with X-ray ionization source [20]. The choice of these substances allows the direct comparison of the data which were received within this study with the data previously described in the literature. Moreover, methyl salicylate forms positive and negative ions simultaneously in air at ambient pressure, offering insight into both negative and positive ion chemistry.

3. Results and Discussion

3.1 Peaks of positive [RIP(+)] and negative [RIP(-)] reactant ions.

Positive and negative reactant ions are responsible for the chemical ionization of analytes and hence for the formation of specific analyte ions. Therefore, both the nature and the formation efficiency of these species play a crucial role in the ion-mobility based methods. The formation of positive and negative reactant ions using ^{63}Ni ionization source as well as the subsequent analyte ionization pathways are well investigated. In air and at ambient pressure, the main positive and negative reactant ions are considered to be $H^+(H_2O)_n$ and $O_2^-(H_2O)_n$, respectively [9,24]. The formation of positively charged product ions occurs mainly over proton transfer from positive reactant ions to the analyte molecule, whereas the negatively charged product ions are formed mainly over hydride subtraction from analyte ion or, more rarely, over association of an analyte molecule and oxygen ion. The alternative ionization sources, like corona discharge or UV-ionization, provide different ionization chemistry (corona discharge in negative mode) [9]. Therefore, the comparison of the data obtained with different ionization sources is complicated. Despite the attractiveness of radioactive ion source, their application is restricted today due to the regulatory restrictions (e.g., transportation, safety, and waste disposal regulations). Additionally, the radioactive ion source cannot be switched off and the radiation intensity cannot be adjusted to the application demands. Therefore, replacement of radioactive ionization source by nonradioactive alternatives producing the similar reactive/product ions is a challenge for modern ion mobility spectrometry.

In our previous study we have demonstrated that X-ray ionization can be utilized in time of flight ion mobility spectrometry instead of the standard radioactive ion source [20]. The spectra obtained with X-ray ionization source were equal to those produced with standard radioactive source (^3H). The determined limits of detection achieved using X-ray ionization source for

acetone in positive mode and for methyl salicylate in negative mode were found to be comparable to those achieved using radioactive ^{3}H source. Therefore, the X-ray was found to be a promising ionization source for ion mobility spectrometry.

In this study we introduce the utilization of X-ray as an ionization source for differential ion mobility spectrometry for the first time. The X-ray source was connected with DMS over the home-made adapter and was assembled onto the DMS lamp holder instead of the original photoionization lamp.

[Fig. 1]

Fig. 1. The relationships between the peak position on compensation field scale and the separation field strength. Ionization with X-ray source is demonstrated in the top and with ^{63}Ni source in the bottom.

The data recorded in form of two-dimensional dispersion plots are demonstrated in Fig. 1. In dispersion plots, both the compensation and the dispersion fields are varied. This plot gives an overview of signals positions and signals intensities within the whole measured separation field range. Additionally, this figure was produced by subtraction of the values recorded in negative mode (negative ions) from the corresponding values recorded in positive mode (positive ions). Therefore, the signals recorded in the positive mode are presented in positive intensity and signals recorded in negative mode are presented in negative intensity. It is notable that in the measurements with both ionization sources (X-ray and ^{63}Ni) the positions of main signals, which are attributed to RIP(+) and RIP(-), were almost identical. However, an additional signal at compensation fields closed to zero (P1) was observed when X-ray was used as an ionization source (see Fig. 1, top). The nature of this signal is most probable related to the materials used for

the construction of the home made adapter (PEEK and PTFE). Therefore, alternative materials (e.g. ceramic) should be used for the improvement of the X-ray adapter in the future.

The combined relationships between the peak position on compensation field scale (CF) and the separation field strength (SF) for ionization with both ^{63}Ni and with X-ray sources are demonstrated in Fig. 2 (top).

[Fig.2]

Fig. 2. Top: relationship between the peak positions on compensation field scale and the separation field strength for ionization with ^{63}Ni and with X-ray sources. Bottom: relationship between relative peak intensity and separation field strength.

The dependencies of the relative intensities of the RIP(+) and RIP(-) to the separation field strength analyzed for ^{63}Ni and X-ray ionization sources can be found in Fig. 2 (bottom). These dependencies reflect the ion transport efficiency under different field conditions. Generally, the peak height decreases with increase of the separation field (independently of the ion type). The higher the ion mobility is, the greater the ion losses within the filter gap [25]. However, at high separation field strength the kinetic and thermodynamic aspects of ion behavior within the DMS filter region, which are driven by the field-heating effect, should be taken into account. The reason for the field heating process is the conversion of kinetic energy acquired by ions in the applied field to thermal energy on collision with neutrals. The field-heating effect results in increase of the effective temperature of the ion to a temperature exceeding its surroundings. Therefore, at high separation field strength the field heating strongly dictates the ion transmission behavior, since ions may dissociate, forming new ions with different ion mobilities [26].

A very high similarity between these relationships together with the similar peak positions support the assumption that positive and negative reactant ions produced by both ionization

sources have the same nature. The RIP(-) intensity is constantly reduced over the whole analyzed separation field strength range. Because of the strong reduction in the RIP(-) intensity with the increase of the separation field strength, the following analysis of the response of the RIP(-) to the experimental conditions was performed at separation field strength of 75 Td. At this separation field strength the shift of the RIP(-) is satisfactory and the RIP(-) intensity is strong enough for reliable data interpretation. In contrast to that, the intensity of the RIP(+) is almost constant within the separation field strength of 56-85 Td. Therefore, the analysis of the relationships between RIP(+) and the experimental conditions can be performed also at higher [as compared to that of RIP(-)] separation field strengths. Within the separation field strength of 85 to 105 Td the RIP(+) intensity is strongly decreased.

[Fig.3]

Fig. 3. X-ray DMS analysis of methyl salicylate in positive (top) and in negative (bottom) modes at separation field strengths (SF) of 94 and 75 Td, respectively. Blank-corrected spectra were produced by subtraction of blank measurement [0 ppm (v/v)] from corresponding spectra recorded with 10 ppb (v/v) of methyl salicylate in carrier gas.

To prove the role of RIP(+) and RIP(-) in analytes ionization process, the methyl salicylate was added to the carrier gas. Addition of methyl salicylate [10 ppb (v/v)] to the carrier gas gave rise to new peaks at -0.14 Td in positive mode (Fig. 3, top, SF = 94 Td) and at -0.16 Td in negative mode (Fig. 3, bottom, SF=75 Td). Furthermore, the intensities of RIP(+) and RIP(-) were significantly reduced as compared to the corresponding blank measurements [Fig. 3, 0 ppb (v/v)]. Blank-corrected spectra after X-ray DMS analysis of methyl salicylate [10 ppb (v/v)] are shown in Fig. 3 (green line). Formation of new peaks at -0.14 (positive mode) and -0.16 Td (negative mode) with addition of methyl salicylate to the carrier gas is demonstrated by positive intensity at CF values corresponding to that of methyl salicylate peak. At the same time, a peak with negative

intensity at CF values corresponding to both RIP(+) and RIP(-) demonstrates reduction of RIP(+) and RIP(-) intensity. The observed simultaneous changes in peak intensities confirm an ionization of analyte by the reactive ions [RIP(+) and RIP(-)] formed during the X-ray ionization. Based on this observation, RIP(+) and RIP(-) were attributed as positive and negative reactant ion peaks, respectively.

3.2 Influence of filament current and accelerating voltage on intensity of reactant ion positive and reactant ion negative peaks.

Generally, the intensity of X-ray source radiation can be increased by increasing of either filament current (I_h) or accelerating voltage (U_h). The filament current controls the number of electrons bombarding the target material. The accelerating voltage of the X-ray generator determines the maximum energy of the electrons bombarding the target material and, thus, the minimum wavelength that can be obtained. The total intensity of the X-ray white radiation is approximately proportional to the atomic number of the anode target, the filament current, and the square of the accelerating voltage [27]. Therefore, both the filament current and the accelerating voltage directly impact on the X-ray output intensity and, hence, on RIP(+) and RIP(-) intensities.

To examine the influence of operating parameters on the RIP(+) and RIP(-) intensities, experiments with different values of filament current and accelerating voltage were performed. No signal was observed when either the filament current was below 550 mA or accelerating voltage was below 2.25 kV. The increase of accelerating voltage, within the range of 2.25 to 5 kV, results in continuous increase of the RIP(+) and RIP(-) intensities when filament current was within the range of 550 to 650 mA. The similar behaviur was observed when filament current was 700 mA and accelerating voltage was within the range of 2.25 to 4 kV. However, the

following increase of the accelerating voltage resulted to only insignificant increase or even to decrease of RIP(+) and RIP(-) intensities (see Fig. 4, bottom). A possible reason for this phenomenon is as follows. The simultaneous increase of the filament current and accelerating voltage results in increase of X-Ray power and temperature. This leads to increased release of components/impurities out of the materials used for the construction of X-ray adapter (PEEK and PTFE). This assumption is supported by a significant increase of the P1 peak intensity. Because of this reason, the following increase of the filament current and accelerating voltage was not investigated in this study. Contour plots demonstrating the influence of X-ray operating parameters on the intensity of RIP(+) and RIP(-) are demonstrated in Fig. 4 (top).

[Fig.4]

Fig. 4. Relationships between filament current, accelerating voltage, and peak intensity of RIP(+) [left] and RIP(-) [right] peaks**.**

3.3 Influence of separation field on model compounds peaks intensity and position on compensation field.

Separation field has influence on both the position of the peaks on compensation scale and the intensity of the peaks. Increase of the separation field strength results in increased separation between observed peaks (see supporting information, Fig. S-2, top). The strongest effect of the separation field strength on the peak position on compensation field scale was observed for acetone. The relationships between the acetone and methyl salicylate (neg, negative mode) peak positions and separation field strength follow the Type A behavior, which is generally understood to result from repetitive clustering and declustering of an ion with polar neutral species in the transport gas [28]. In both positive and negative modes, dependence of P1 peaks positions follow

Type C behavior, which can be explained on the basis of simple physical impacts with little or no polar interactions or clustering [28]. Dependence of the position of methyl salicylate peak in positive mode (pos, positive mode) on separation field strength follows the Type B behavior, which can be viewed as a combination of Types A and C [28]. It was observed that increase of the separation field strength resulted in strong reduction of the P1 peaks intensities in both positive and negative modes. However, the influence of the separation field strength on intensities of the acetone and methyl salicylate (both modes) peaks was found to be much weaker or even negligible (see supporting information, Fig. S-2, bottom). Interestingly, after a minor decrease of the peak intensity of methyl salicylate in the negative mode at a separation field of about 87 Td the following increase of the peak intensity within the separation field values range of 95 to 105 Td was observed. The similar effect was observed by Maziejuk et al. during the analysis of methyl salicylate with DMS of different construction [29]. This phenomenon was explained by Nazarov et al. [23]. Using DMS-MS coupling, they have confirmed the formation of different methyl salicylate (MS) product ions under different separation field conditions. It was found that the transition from $MS(O_2)^-$ to $(MS-H)^-$ occurs within the separation field range of 100 to 110 Td. These observations are in good agreement with the findings achieved in this study. The nature of this transition can be explained in terms of increased collision energy or increased effective temperature [23].

The peak of acetone is well separated from other peaks, therefore the analysis of acetone can be performed at usual for DMS analysis separation field of 94 Td. However, because of the poor resolution between the peaks of methyl salicylate ions and P1 peaks (especially in positive mode) the following analysis of methyl salicylate was performed at a higher separation field strength of

114 Td. At this separation field strength the intensity of P1 peaks is reduced in almost two times as compared to those at 94 Td. However, in addition to the improved resolution, minor (positive mode) to no (negative mode) decrease of methyl salicylate peaks intensity was observed when separation field strength was increased from 94 to 114 Td.

3.4 Determination of analytical parameters for the model compounds analyzed by X-ray DMS and ^{63}Ni-DMS.

In order to prove the efficiency of X-ray as an ionization source for DMS the analytical parameters obtained with X-ray DMS where compared with those obtained with traditional ^{63}Ni-DMS. The summarized compensation field (CF) values and limits of detection for model analytes obtained with X-ray and ^{63}Ni-ionization sources can be found in Table 1. Limits of detection were calculated according to the concentration of the analyte in the carrier gas entering the ion source and in accordance with DIN 32645 [30].

Table 1. Compensation field (CF) values and limits of detection (LOD) for model substances as well as CF for RIP(+) and RIP(-) achieved with X-ray and ^{63}Ni ionization sources.

	X-ray DMS [a]		^{63}Ni-DMS	
	CF [Td]	LOD [$ppb_{v/v}$]	CF [Td]	LOD [$ppb_{v/v}$]
MS (pos) [b]	-0.13	1.39	-0.14	0.84
MS (neg) [b]	-0.41	1.52	-0.42	0.68
Acetone (pos) [c]	-0.80	0.17	-0.78	0.12
RIP(+) [c]	-1.27		-1.28	
RIP(-) [c]	-1.91		-1.92	

[a] Accelerating voltage = 4.5 kV, filament current = 650 mA

[b] Separation field = 94 Td

[c] Separation field = 114 Td

A non-linear relationship between signal area and concentration common for non-direct ionization mechanisms (e.g. APCI) was observed for both model compounds when X-ray and ^{63}Ni were used as ionization sources [9,13,31]. Additionally, calibration of acetone was complicated due to significant dimer formation at concentrations higher than approximately 3 $ppb_{v/v}$. Representative differential mobility spectra of methyl salicylate at different concentrations are exemplarily presented in Fig. 5.

[Fig. 5]

Fig. 5. Differential mobility spectra of methyl salicylate at different concentrations recorded in positive (top, positive ions) and negative (bottom, negative ions) modes at separation field strength of 114 Td, filament current of 650 mA, and accelerating voltage of 4.5 kV. Dependences of the signal intensity on the concentration are presented in the inserts.

The LOD values for acetone and methyl salicylate obtained with X-ray DMS were found to be 1.5 to 2.2 times higher as compared to those obtained with standard ^{63}Ni-source and in the hundreds-of-parts-per-trillion to parts-per-billion range (v/v, concentration of the analyte in the carrier gas entering the ion source).

It should be noted that the sample introduction for measurements performed by X-ray DMS and ^{63}Ni-DMS was realized differently. In contrast to the measurements performed by ^{63}Ni-DMS, in which the carrier gas was introduced into DMS via the standard inlet, the introduction of carrier

gas for the measurements performed by X-ray was realized via a home-built adapter. This adapter was assembled onto the DMS lamp holder instead of the original photoionization lamp. The introduction via lamp holder was necessary to provide much faster (as compared to standard inlet) transport of ions into the DMS filter (separation) region. However, the distance between the ionization region and the filter region is still much higher as compared to the DMS with ^{63}Ni ionization source, where the ionization source is located directly on the DMS chip. Additionally, as it was demonstrated in previous sections (see Figures 1 and 4) the release of components/impurities out of the materials used for the construction of X-ray adapter can affect the efficiency of ionization. The optimization of the sample introduction system as well as the proper choice of materials for the X-ray adapter may decrease the detection limits. Nevertheless, even the LOD values achieved with the current experimental setup are competitive with those calculated for DMS equipped with traditional ^{63}Ni radioactive ionization source (see Table 1).

The representative differential mobility spectra obtained with X-ray and ^{63}Ni-ionization sources are demonstrated on example of methyl salicylate (c = 10 ppb v/v) in Fig. 6.

[Fig. 6]

Fig. 6. Differential mobility spectra of methyl salicylate (10 $ppb_{v/v}$) obtained with X-ray, and ^{63}Ni-ionization sources in positive (top, positive ions) and negative (bottom, negative ions) modes at separation field strength of 114 Td, filament current of 650 mA, and accelerating voltage of 4.5 kV.

4. Conclusion

The X-ray ionization source has been found to be a suitable ionization source for differential ion mobility spectrometry. An attractive feature of the X-ray source is the possibility to adjust the

radiation intensity to the application demands by varying of the experimental parameters, e.g. filament current or accelerating voltage. X-rays are a type of ionizing radiation and, therefore, X-ray sources should be constructed and used according to the corresponding safety directives and regulations.[32] However, in contrast to the radioactive sources (^{63}Ni, ^{3}H, ^{241}Am), the X-ray source can be switched of enabling safe transportation of the device. The recorded with X-ray DMS spectra in both positive and negative modes were equivalent to those observed using standard ^{63}Ni-radioactive source. This is especially notable for the reactive ions formed in negative mode, because the chemistry provided by other nonradioactive sources in the negative mode is more complicated or even different than that observed with a ^{63}Ni source. The analysis of the model compounds demonstrates that the sensitivity of a home-built and only partially optimized X-ray DMS setup is already competitive with a commercially available ^{63}Ni-DMS system. LODs within the hundreds-of-parts-per-trillion to parts-per-billion range were achieved (concentration of the analyte in the carrier gas entering the ion source). Further improvements and optimization may significantly increase the sensitivity of X-ray DMS. In future, X-ray may be especially an attractive alternative to radioactive sources (e.g. ^{63}Ni or ^{3}H) for on-line (and on-site) monitoring.

Appendix A. Supporting information

Supplementary data associated with this article can be found in the online version at

References

[1] A.A. Shvartsburg, Differential Ion Mobility Spectrometry: Nonlinear Ion Transport and Fundamentals of FAIMS, CRC Press, Boca Raton, 2008.

[2] B.M. Kolakowski, Z. Mester, Review of applications of high-field asymmetric waveform ion mobility spectrometry (FAIMS) and differential mobility spectrometry (DMS), Analyst 132 (2007) 842-864. http://dx.doi.org/10.1039/b706039d

[3] E.V. Krylov, E.G. Nazarov, Electric field dependence of the ion mobility, Int. J. Mass Spectrom. 285 (2009) 149-156. http://dx.doi.org/10.1016/j.ijms.2009.05.009

[4] I.A. Buryakov, E.V. Krylov, E.G.Nazarov, U.Kh. Rasulev, A new method of separation of multi-atomic ions by mobility at atmospheric pressure using a high-frequency amplitude-asymmetric strong electric field, Int. J. Mass Spectrom. Ion Process. 128 (1993) 143-148. http://dx.doi.org/10.1016/0168-1176(93)87062-W

[5] R.A. Miller, E.G. Nazarov, G.A. Eiceman, A.T. King, A MEMS radio-frequency ion mobility spectrometer for chemical vapor detection, Sensors and Actuators A: Physical 91 (2001) 301-312. http://dx.doi.org/10.1016/S0924-4247(01)00600-8

[6] B.B. Schneider, T.R. Covey, S.L. Coy, E.V. Krylov, E.G. Nazarov, Planar differential mobility spectrometer as a pre-filter for atmospheric pressure ionization mass spectrometry, Int. J. Mass Spectrom. 298 (2010) 45-54. http://dx.doi.org/10.1016/j.ijms.2010.01.006

[7] B.B. Schneider, T.R. Covey, E.G. Nazarov, DMS-MS separations with different transport gas modifiers, Int. J. Ion Mobil. Spec. 16 (2013) 207-216. http://dx.doi.org/10.1007/s12127-013-0130-8

[8] F. Liang, K. Kerpen, A. Kuklya, U. Telgheder, Fingerprint identification of volatile organic compounds in gasoline contaminated groundwater using gas chromatography differential ion mobility spectrometry, Int. J. Ion Mobil. Spec. 15 (2012) 169-177. http://dx.doi.org/10.1007/s12127-012-0101-5

[9] D.S. Levin, P. Vouros, R.A. Miller, E.G. Nazarov, Using a Nanoelectrospray-Differential Mobility Spectrometer-Mass Spectrometer System for the Analysis of Oligosaccharides with

Solvent Selected Control Over ESI Aggregate Ion Formation, J. Am. Soc. Mass Spectrom. 18 (2007) 502-511. http://dx.doi.org/10.1016/j.jasms.2006.10.008

[10] G.A. Eiceman, Z. Karpas, H.H. Hill Jr., Ion Mobility Spectrometry, Third Edition, CRC Press, 2014.

[11] I.A. Buryakov, E.V. Krylov, E.G.Nazarov, U.Kh. Rasulev, A new method of separation of multi-atomic ions by mobility at atmospheric pressure using a high-frequency amplitude-asymmetric strong electric field, Int. J. Mass Spectrom. Ion Process. 128 (1993) 143-148. http://dx.doi.org/10.1016/0168-1176(93)87062-W

[12] E.G. Nazarov, R.A. Miller, G.A. Eiceman, J.A. Stone, Miniature Differential Mobility Spectrometry Using Atmospheric Pressure Photoionization, Anal. Chem. 78 (2006) 4553-4563. http://dx.doi.org/10.1021/ac052213i

[13] A. Kuklya,; C. Engelhard, F. Uteschil, K. Kerpen, R. Marks, U. Telgheder, Low-Temperature Plasma Ionization Differential Ion Mobility Spectrometry, Anal Chem. 87 (2015) 8932-8940. http://dx.doi.org/10.1021/acs.analchem.5b02077

[14] D. Zhao, J. Jia, J. Li, J. Li, X. Gao, X. He, Corona Discharge Ionization Source for a Planar High-Field Asymmetric Waveform Ion Mobility Spectrometer, Anal. Lett. 46 (2013) 452-460. http://dx.doi.org/10.1080/00032719.2012.725190

[15] C.A. Hill, C.L.P. Thomas, A pulsed corona discharge switchable high resolution ion mobility spectrometer-mass spectrometer, Analyst 128 (2003) 55-60. http://dx.doi.org/10.1039/B207558J

[16] K. Sekimoto, M. Takayama, Influence of needle voltage on the formation of negative core ions using atmospheric pressure corona discharge in air, Int. J. Mass Spectrom. 261 (2007) 38-44. http://dx.doi.org/10.1016/j.ijms.2006.07.027

[17] M. Sabo, J. Matúška, S. Matejčík, Specific O_2^- generation in corona discharge for ion mobility spectrometry, Talanta 85 (2011) 400-405. http://dx.doi.org/10.1016/j.talanta.2011.03.074

[18] H. Borsdorf, E.G. Nazarov, G.A. Eiceman, Atmospheric pressure chemical ionization studies of non-polar isomeric hydrocarbons using ion mobility spectrometry and mass spectrometry with different ionization techniques, J. Am. Soc. Mass Spectrom. 13 (2002) 1078-1087. http://dx.doi.org/10.1016/S1044-0305(02)00429-4

[19] M.J. Waltman, P. Dwivedi, H.H. Hill Jr, W.C. Blanchard, R.G. Ewing, Characterization of a distributed plasma ionization source (DPIS) for ion mobility spectrometry and mass spectrometry, Talanta 77 (2008) 249-255. http://dx.doi.org/10.1016/j.talanta.2008.06.014

[20] T. Reinecke, A.T. Kirk, A. Heptner, D. Niebuhr, S. Böttger, S. Zimmermann, A compact high-resolution X-ray ion mobility spectrometer, Rev. Sci. Instrum. 87 (2016) 053120. http://dx.doi.org/10.1063/1.4950866

[21] V.S. Pershenkov, A.D. Tremasov, V.V. Belyakov, A.U. Razvalyaev, V.S. Mochkin, X-ray ion mobility spectrometer, Microelectron. Reliab. 46 (2006) 641-644. http://dx.doi.org/10.1016/j.microrel.2005.07.003

[22] M. Wojdyr, J. Appl. Cryst., Fityk: a general-purpose peak fitting program, 43 (2010) 1126-1128. http://dx.doi.org/10.1107/S0021889810030499

[23] E.G. Nazarov, S.L. Coy, E.V. Krylov, R.A. Miller, G.A. Eiceman, Pressure Effects in Differential Mobility Spectrometry, Anal. Chem. 78 (2006) 7697-7706. http://dx.doi.org/10.1021/ac061092z

[24] C. J. Hayhurst, P. Watts, A. Wilders, Studies on gas-phase negative ion/molecule reactions of relevance to ion mobility spectrometry: mass analysis and ion identification of the negative

reactant ion peak in “clean” air, Int. J. Mass Spectrom. Ion Processes, 121 (1992) 127-139. http://dx.doi.org/10.1016/0168-1176(92)80076-D

[25] E.V. Krylov, E.G. Nazarov, R.A. Miller, Differential mobility spectrometer: Model of operation, Int. J. Mass Spectrom. 266 (2007) 76-85. http://dx.doi.org/10.1016/j.ijms.2007.07.003

[26] A. Wilks, M. Hart, A. Koehl, J. Somerville, B. Boyle, D. Ruiz-Alonso, Characterization of a miniature, ultra-high-field, ion mobility spectrometer, Int. J. Ion Mobil. Spec. 15 (2012) 199-222. http://dx.doi.org/10.1007/s12127-012-0109-x

[27] R.E. Dinnebier, S.J.L. Billinge, Powder Diffraction: Theory and Practice, RSC Publishing, 2008.

[28] B.B. Schneider, E.G. Nazarov, F. Londry, P. Vouros, T.R. Covey, Mass. Spectrom. Rev., in press. http://dx.doi.org/10.1002/mas.21453

[29] M. Maziejuk, W. Lisowski, M. Szyposzyńska, T. Sikora, A. Zalewska, Differential Ion Mobility Spectrometry in Application to the Analysis of Gases and Vapours, Solid State Phenomena 223 (2015) 283-290. http://dx.doi.org/10.4028/www.scientific.net/SSP.223.283

[30] Deutsches Institut für Normung e. V (DIN). DIN 32645:2008-11, Berlin, 2008. Chemical analysis - Decision limit, detection limit and determination limit under repeatability conditions - Terms, methods, evaluation.

[31] A. Kuklya, F. Uteschil, K. Kerpen, R. Marks, U. Telgheder, Development of an electrospray-^{63}Ni-differential ion mobility spectrometer for the analysis of aqueous samples, Talanta 120 (2014) 173-180. http://dx.doi.org/10.1016/j.talanta.2013.10.056

[32] Official Journal of the European Union, Directive 2013/59/Euratom - protection against ionising radiation

Highlights

- X-ray is used as an ionization source for DMS for the first time.
- RIP and RIN peaks are identical for X-ray and ^{63}Ni ion sources.
- Experimental parameters were successfully optimized.
- LOD values achieved with X-ray and ^{63}Ni sources are comparable.
- Non-radioactive X-ray ionization source increases the range of DMS applications.

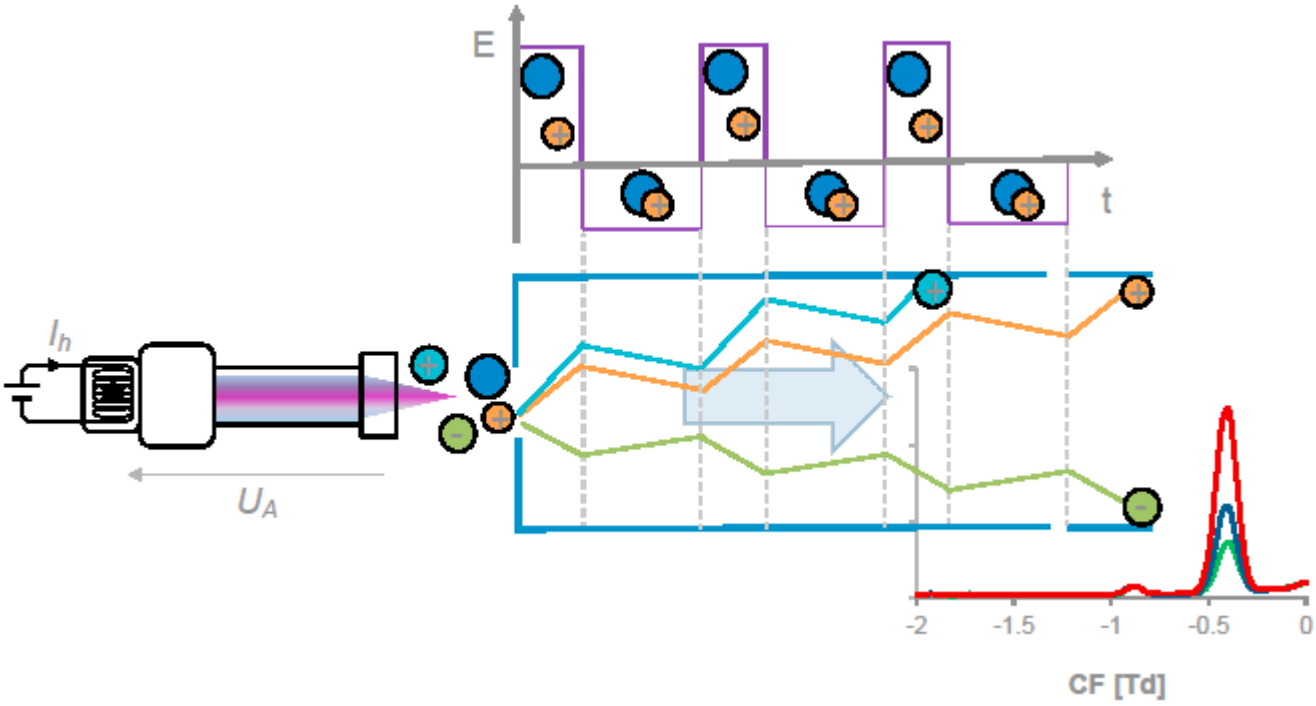

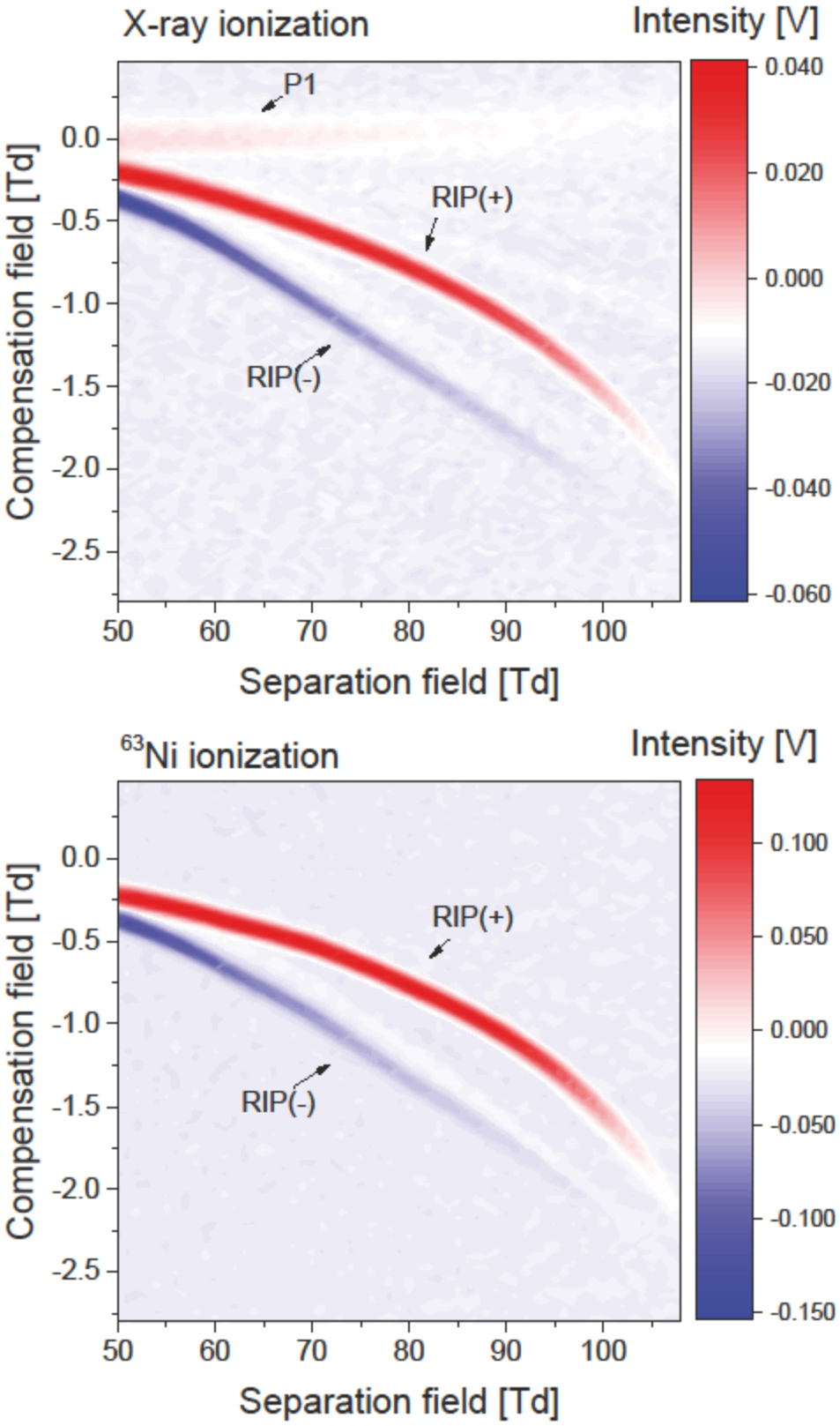
X-ray ionization
Intensity [V]
P1
RIP(+)
RIP(-)
Compensation field [Td]
Separation field [Td]
0.040
0.020
0.000
-0.020
-0.040
-0.060
63Ni ionization
Intensity [V]
RIP(+)
RIP(-)
Compensation field [Td]
Separation field [Td]
0.100
0.050
0.000
-0.050
-0.100
-0.150

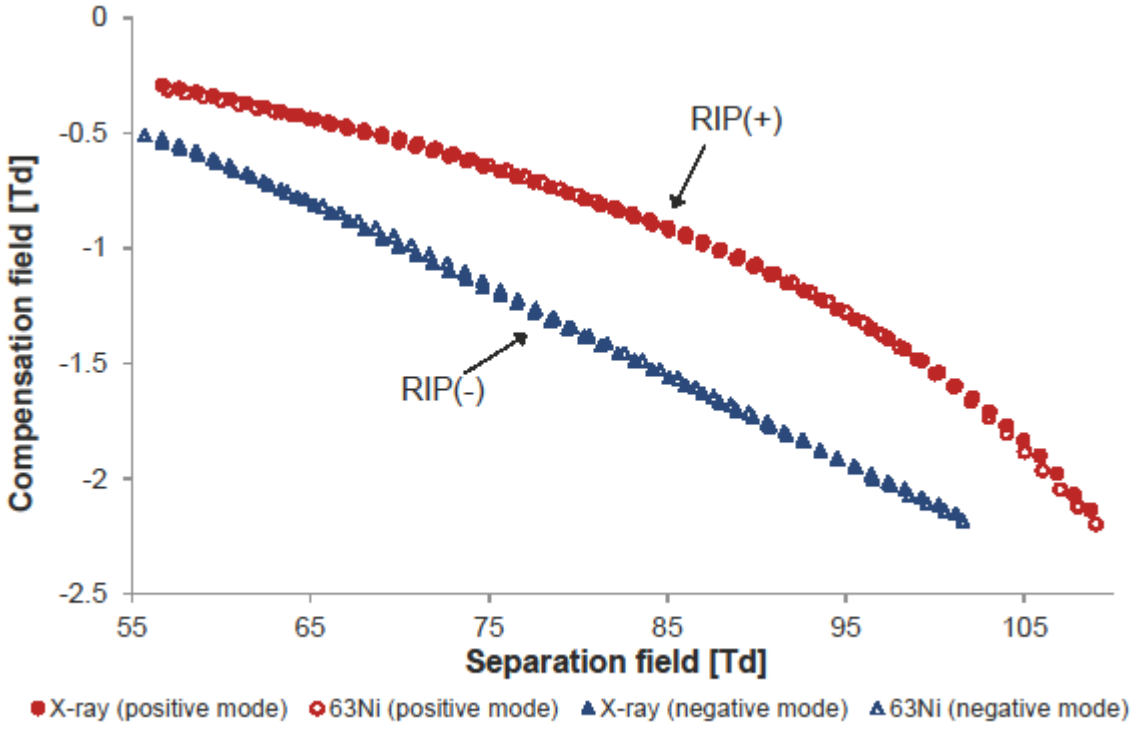
0
-0.5
-1
-1.5
-2
-2.5
Compensation field [Td]
RIP(+)
RIP(-)
55
65
75
85
95
105
Separation field [Td]
X-ray (positive mode)
63Ni (positive mode)
X-ray (negative mode)
63Ni (negative mode)

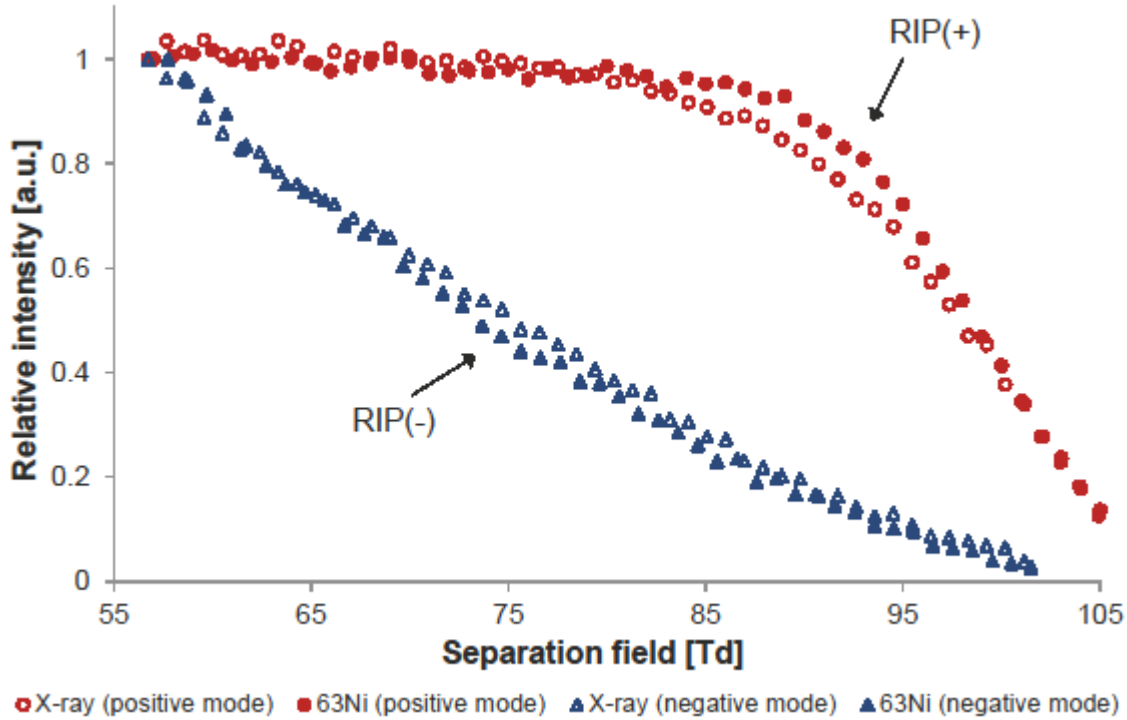
1
0.8
0.6
0.4
0.2
0
Relative intensity [a.u.]
RIP(+)
RIP(-)
55
65
75
85
95
105
Separation field [Td]
X-ray (positive mode)
63Ni (positive mode)
X-ray (negative mode)
63Ni (negative mode)

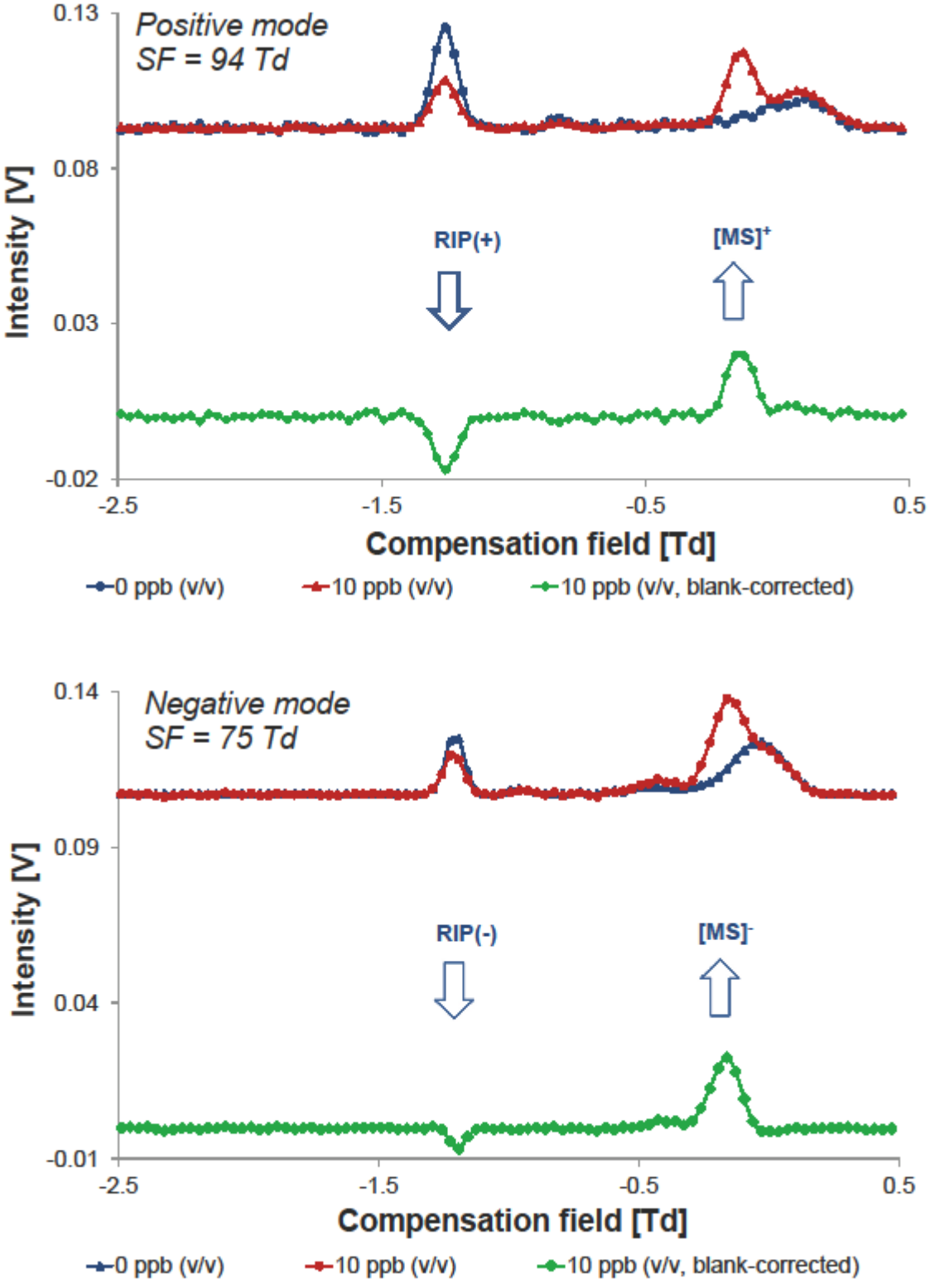
Positive mode
SF = 94 Td
0.13
0.08
0.03
-0.02
Intensity [V]
RIP(+)
[MS]+
-2.5
-1.5
-0.5
0.5
Compensation field [Td]
0 ppb (v/v)
10 ppb (v/v)
10 ppb (v/v, blank-corrected)
Negative mode
SF = 75 Td
0.14
0.09
0.04
-0.01
Intensity [V]
RIP(-)
[MS]-
-2.5
-1.5
-0.5
0.5
Compensation field [Td]
0 ppb (v/v)
10 ppb (v/v)
10 ppb (v/v, blank-corrected)

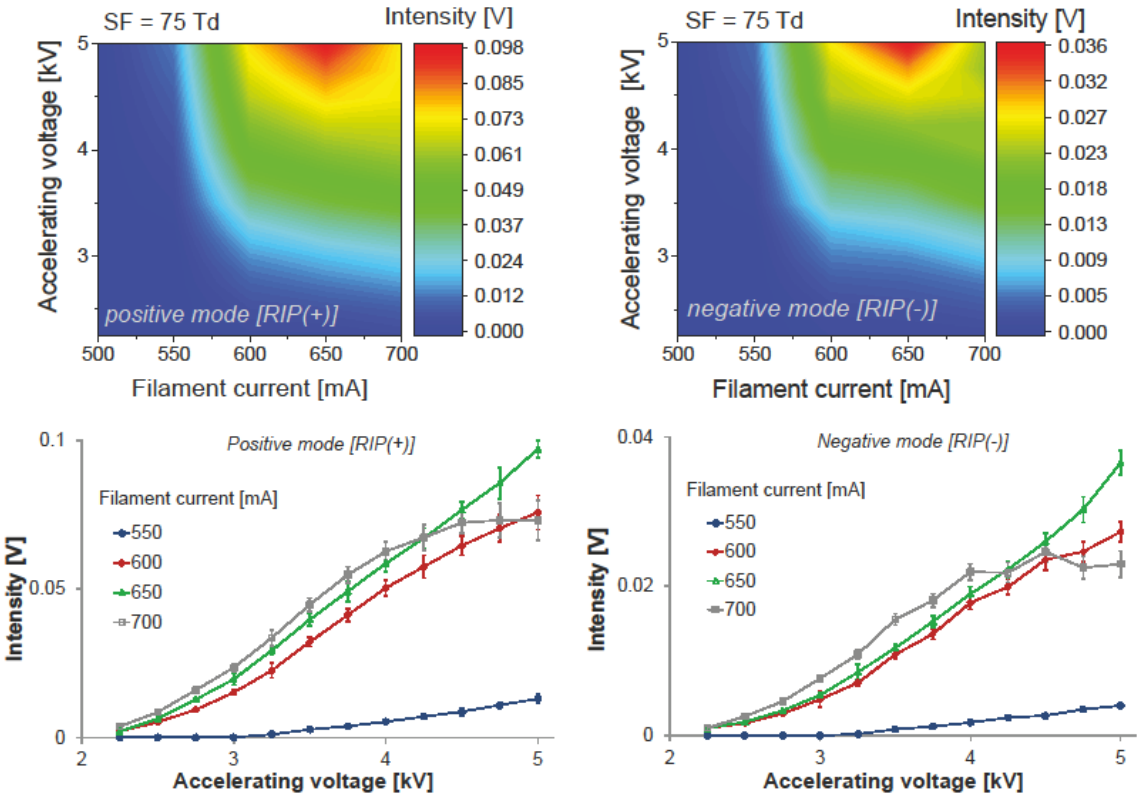
SF = 75 Td
Intensity [V]
Accelerating voltage [kV]
positive mode [RIP(+)]
Filament current [mA]
negative mode [RIP(-)]
Positive mode [RIP(+)]
Negative mode [RIP(-)]
550
600
650
700
Intensity [V]
Accelerating voltage [kV]

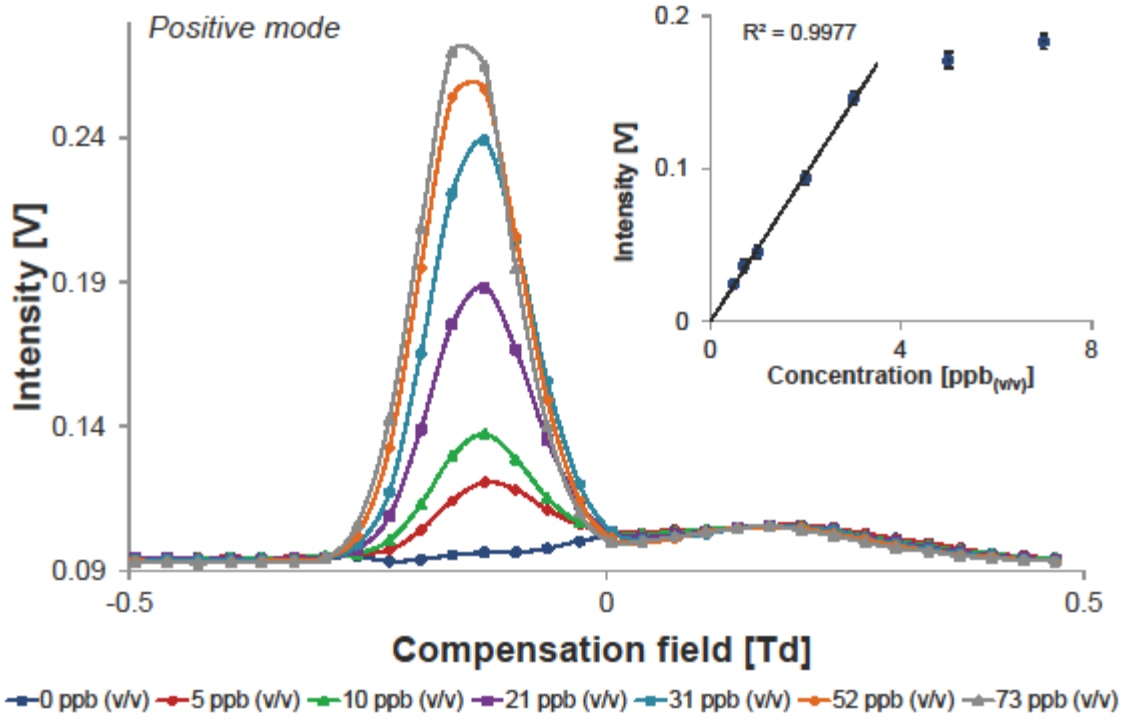
Positive mode
Intensity [V]
0.24
0.19
0.14
0.09
-0.5
0
0.5
Compensation field [Td]
R² = 0.9977
0.2
0.1
0
0
4
8
Concentration [ppb(v/v)]
0 ppb (v/v)
5 ppb (v/v)
10 ppb (v/v)
21 ppb (v/v)
31 ppb (v/v)
52 ppb (v/v)
73 ppb (v/v)

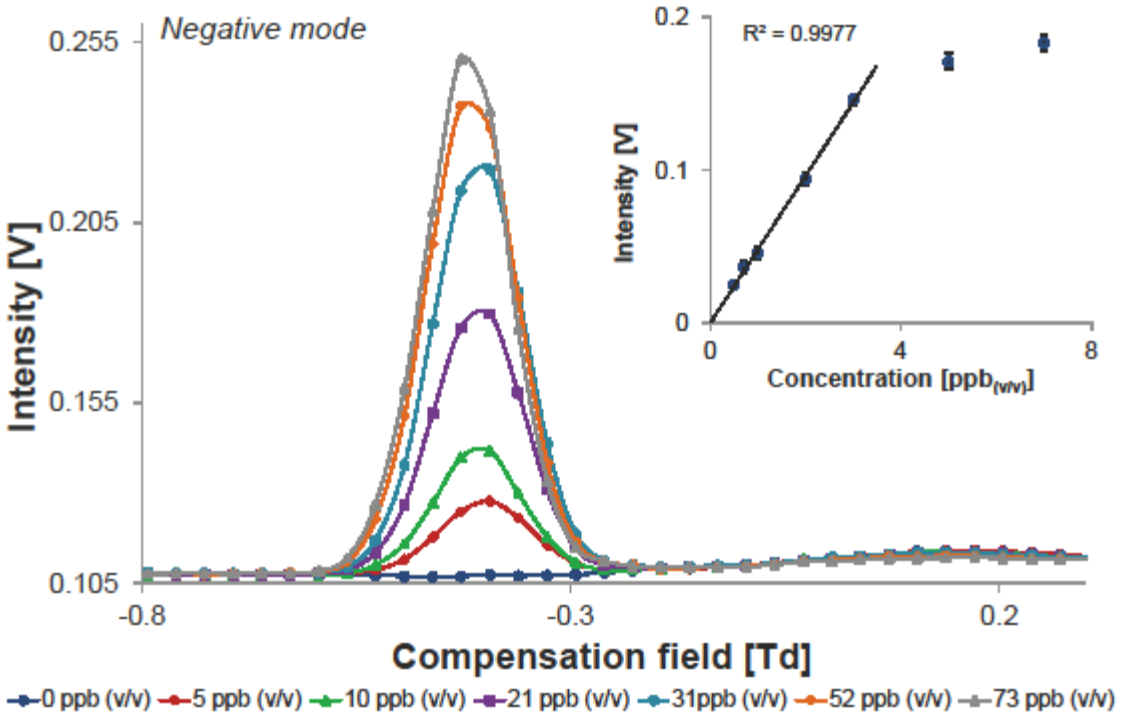
Negative mode
Intensity [V]
0.255
0.205
0.155
0.105
-0.8
-0.3
0.2
Compensation field [Td]
R² = 0.9977
0.2
0.1
0
0
4
8
Concentration [ppb(v/v)]
0 ppb (v/v)
5 ppb (v/v)
10 ppb (v/v)
21 ppb (v/v)
31ppb (v/v)
52 ppb (v/v)
73 ppb (v/v)

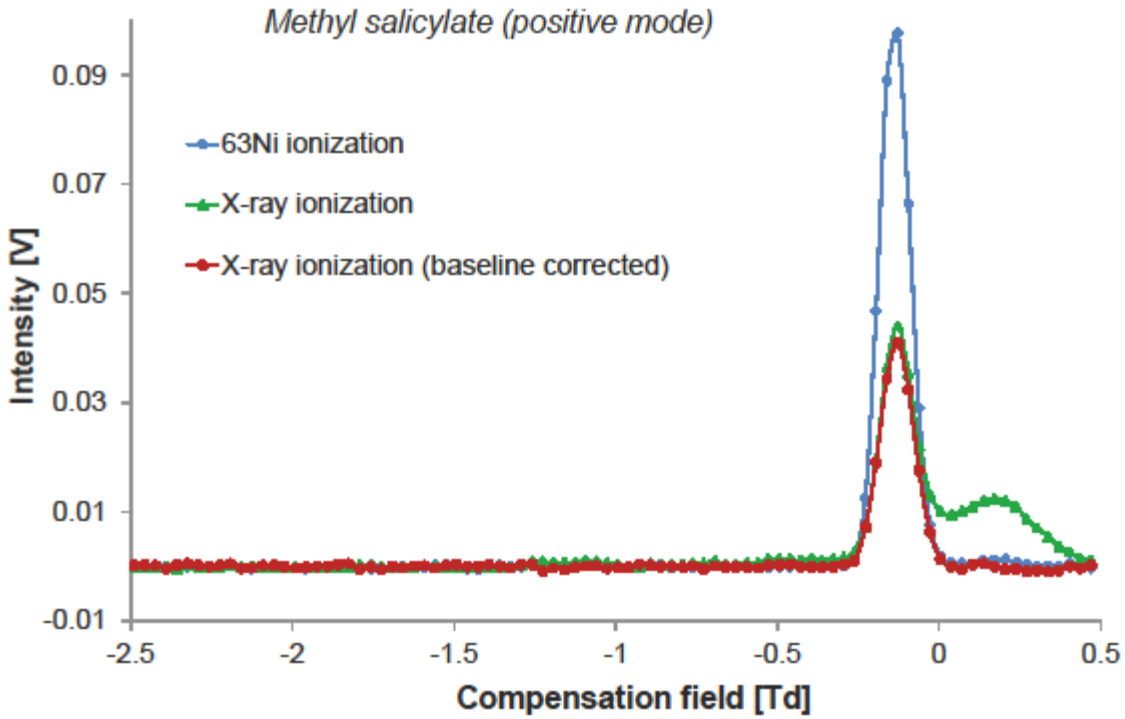
Methyl salicylate (positive mode)
63Ni ionization
X-ray ionization
X-ray ionization (baseline corrected)
Intensity [V]
0.09
0.07
0.05
0.03
0.01
-0.01
-2.5
-2
-1.5
-1
-0.5
0
0.5
Compensation field [Td]

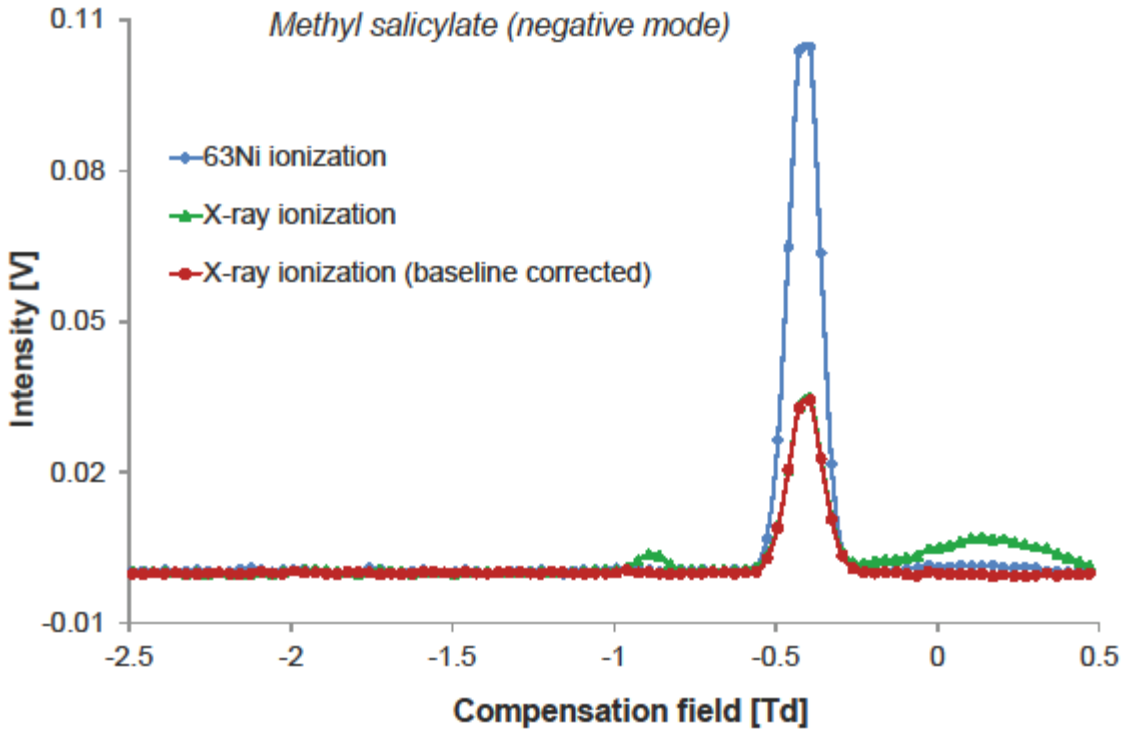
Methyl salicylate (negative mode)
63Ni ionization
X-ray ionization
X-ray ionization (baseline corrected)
Intensity [V]
0.11
0.08
0.05
0.02
-0.01
-2.5
-2
-1.5
-1
-0.5
0
0.5
Compensation field [Td]

X-ray ionization differential ion mobility spectrometry

Kuklya, Andriy; Reinecke, Tobias; Uteschil, Florian; Kerpen, Klaus; Zimmermann, Stefan; Telgheder, Ursula

DOI: https://doi.org/10.1016/j.talanta.2016.10.024

URN: urn:nbn:de:hbz:464-20190319-105553-4

Link: https://duepublico.uni-duisburg-essen.de:443/servlets/DocumentServlet?id=48402

Source: This is the "Authors Accepted Manuscript" of an article published in: Talanta, Volume 162, 2017, Pages 159-166; Available online 4 October 2016. The final version may be found at: https://doi.org/10.1016/j.talanta.2016.10.024